Letter

Frozen autocatalytic fronts in a radial flow

L. Negrojević, A. Comolli, Fabian Brau,* and A. De Wit†
Nonlinear Physical Chemistry Unit, Université Libre de Bruxelles (ULB), CP231, 1050 Bruxelles, Belgium

(Received 16 July 2024; accepted 16 October 2024; published 20 November 2024)

Autocatalytic reaction-diffusion fronts are localized reaction zones propagating at a constant speed with a constant width. We show both theoretically and experimentally that, if the reactant Y of the autocatalytic reaction is injected radially at a constant flow rate in a sea of the autocatalytic species X, a stationary front can be maintained at a fixed position that scales linearly with the flow rate. When this reaction front is about to reach a stationary state, a second outward traveling front emerges to adapt the outer concentration of the autocatalytic species to the stoichiometry ratio between X and Y. Simple analytical solutions to the reaction-diffusion-advection equations governing the dynamics are computed for both fronts. The analytical predictions for the stationary front position and moving front dynamics as a function of injection flow rate, reactant concentration, and gap of the quasi-two-dimensional reactor agree well with experimental results obtained with the autocatalytic chlorite-tetrathionate reaction.

DOI: 10.1103/PhysRevResearch.6.L042044

Propagating reaction-diffusion (RD) fronts are encountered in numerous applications in biological [1] or chemical [2,3] systems, including disease spreading [4], polymerization [5], and many others. They correspond to a localized zone of reaction that propagates via diffusion when initially separated regions containing different reactants are put in contact. Among various types of fronts, autocatalytic fronts arise when one of the reactants catalyzes its own production. When coupled with diffusion, this localized autocatalytic reaction produces a front that travels with a constant shape and velocity [2,3,6–8].

In the presence of advective flows with a constant velocity, the speed and shape of such autocatalytic fronts can be modified, as observed in cylindrical tubes and quasi-two-dimensional (2D) reactors [9–12]. In advective flows adverse to the direction of their propagation, static autocatalytic fronts can be observed if the magnitude of the RD propagation velocity matches the opposing flow velocity, as observed in laminar flows [13]. In heterogeneous porous media or flows around obstacles, autocatalytic fronts can become frozen with various shapes in adverse rectilinear flows due to the pinning of the front in low-velocity zones around the obstacles [14–16].

The situation is, however, more complex in radial flows, where the fact that the velocity decreases along the radius impacts the dynamics of the front when the autocatalytic species is injected into the reactant at a constant flow rate [17]. Interest has therefore developed in understanding the dynamics of radially moving chemical fronts in the presence of passive advection [17–21], in connection with applications such as spreading of pollution in porous media [22], CO_2 mineralization [18], or mixing efficiency [23], for instance.

In this context, we show both theoretically and experimentally that static, frozen fronts can be maintained at a fixed distance from the injection port when the reactant of an autocatalytic reaction is injected in a sea of the autocatalytic species via a nonhomogeneous radial flow field. The radial position of this frozen front scales linearly with the flow rate and can also be controlled by the thickness of the solution layer and the concentration of the reactant. Such frozen fronts of programmable radial position offer a novel way of confining gradient sources to analyze localized pattern formation [24,25]. In parallel, a second traveling front escapes out of the reactive stationary front to adapt the initial outer concentration of X to its stoichiometry ratio with Y. We characterize the analytical temporal evolution of both fronts' properties, including the concentration profiles, the front position and width, the reaction rate, and the total amount of the autocatalyst formed. We further show an excellent agreement between the theoretical predictions and experimental data obtained by injecting the reactant mixture of the autocatalytic chlorite-tetrathionate (CT) reaction into a quasi-2D reactor initially filled with the autocatalytic species.

We consider a 2D system filled with species X at an initial concentration $\bar{x}_0$ in which the reactant Y of the autocatalytic $2X + Y \rightarrow 3X$ reaction in concentration $\bar{y}_0$ is injected radially at a constant flow rate $\bar{Q}$ [Fig. 1(a)]. The equations governing the reaction-diffusion-advection (RDA) dynamics read

$$\partial_{\bar{t}}\bar{x} + \vec{v}\cdot\bar{\nabla}\bar{x} = \bar{D}\bar{\nabla}^2\bar{x} + n\,\bar{k}\,\bar{x}^2\,\bar{y}, \tag{1a}$$

$$\partial_{\bar{t}}\bar{y} + \vec{v}\cdot\bar{\nabla}\bar{y} = \bar{D}\bar{\nabla}^2\bar{y} - \bar{k}\,\bar{x}^2\,\bar{y}, \tag{1b}$$

*Contact author: fabian.brau@ulb.be
†Contact author: anne.de.wit@ulb.be

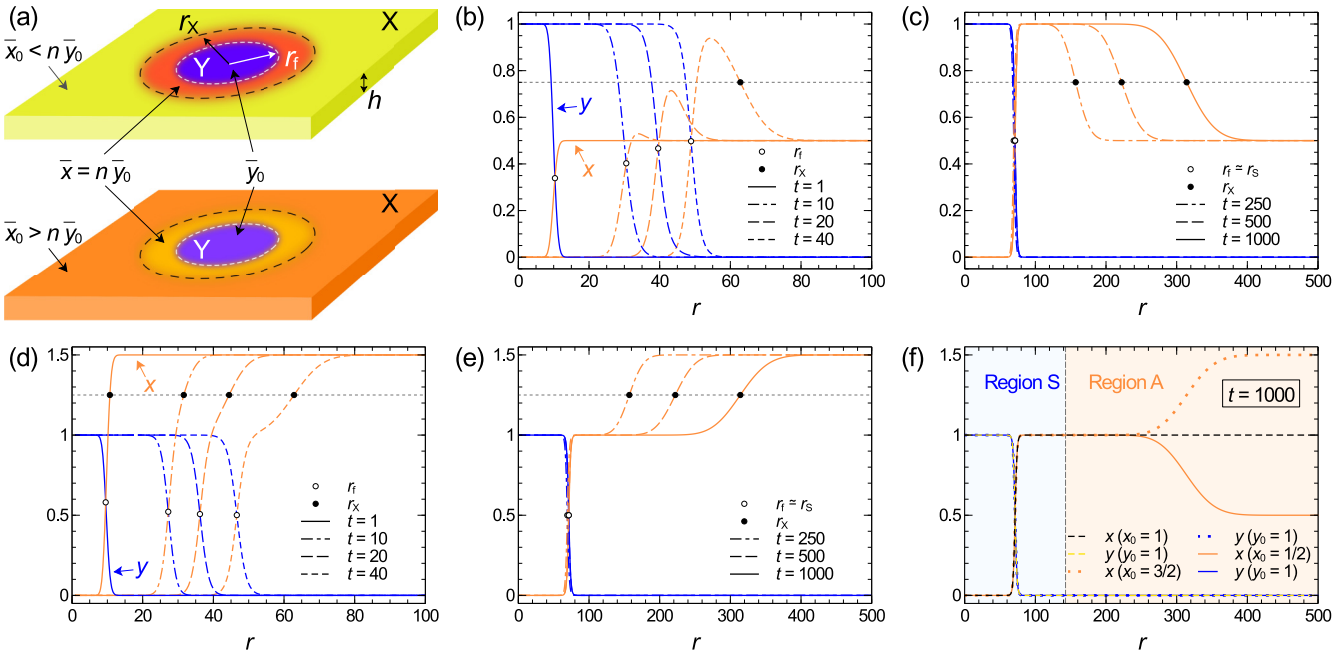

FIG. 1. (a) Schematic of a quasi-2D reactor of thickness h filled with the autocatalytic species X in which the reactant Y is radially injected at a constant flow rate Q. (b), (c) Numerical concentration profiles obtained by solving Eqs. (2) with $y_0 = n = 1$, $x_0 = 1/2 < n$, and $Q = 50$. (b) The local increase of x near the reaction front localized at $r = r_f$ continues until $x = n = 1$ ($\bar{x} = n\bar{y}_0$), leading to a frozen reaction front at some radial position $r_f = r_S$ (c). The horizontal dashed lines correspond to the concentration $(x_0 + n)/2$ used to define r_X. The local excess of X with respect to the bulk is then advected outward [see top panel of (a)]. (d), (e) Same as (b) and (c) for $x_0 = 3/2 > n$ with the adaptation of x to n upon feeding of Y up to the stationary position and outward advection of the local depletion of X with respect to the bulk [see bottom panel of (a)]. (f) Comparison between the concentration profiles of X and Y displayed in (c) and (e) at $t = 1000$ together with the concentration profiles for $x_0 = 1 = n$ and the two regions, "S" for stationary and "A" for advected.

where $\bar{x}$ and $\bar{y}$ are the concentrations of X and Y, respectively, $\bar{D}$ is their diffusion coefficient, $\bar{k}$ is the kinetic constant, and n the stoichiometric ratio between X and Y. For example, $n = 1$ corresponds to the iodate-arsenous acid reaction [26] and $n = 6$ to the CT reaction [8]. Assuming flow incompressibility and radial symmetry, the velocity field $\vec{v}$ varies only with the radius $\bar{r}$ as $\vec{v}(\bar{r}) = \bar{Q}/(2\pi\bar{h}\bar{r})\,\vec{e}_r$, where $\bar{Q}$ is the injection flow rate, and $\bar{h}$ is the height of the reactor. Equations (1) are nondimensionalized by rescaling $\bar{x}$ by $\bar{y}_0$, $\bar{y}$ by $\bar{y}_0/n$, time by $\bar{\tau} = 1/\bar{k}\bar{y}_0^2$, and lengths by $\bar{\ell} = \sqrt{\bar{D}\bar{\tau}}$,

$$\partial_t x + \frac{Q-1}{r}\partial_r x = \partial_r^2 x + x^2 y, \tag{2a}$$

$$\partial_t y + \frac{Q-1}{r}\partial_r y = \partial_r^2 y - x^2 y, \tag{2b}$$

where $Q = \bar{Q}/2\pi\bar{h}\bar{D}$ and quantities without a bar are dimensionless. These equations are solved with initial conditions $x(r,0) = x_0\,H(r)$, $y(r,0) = n\,H(-r)$, where $H(\cdot)$ is the Heaviside function, and boundary conditions (BCs) $x(0,t) = y(\infty,t) = 0$, $x(\infty,t) = x_0$, and $y(0,t) = n$.

Figure 1 shows typical spatiotemporal evolutions of the concentration profiles obtained by solving Eqs. (2) numerically. Upon injection, Y invades advectively X and, if $x_0 < n$ [Figs. 1(b) and 1(c)], the concentration of X increases to adapt to the stoichiometric ratio n in the reaction zone located at a position $r = r_f(t)$. Once the outward advective supply of Y starts to be counterbalanced by its inward natural consumption by the RD front, the reaction zone stops moving and a stationary frozen RDA front is obtained at a fixed radial position $r_f = r_S$ [Fig. 1(c)]. The autocatalytic reaction continues to produce X dynamically in the stationary front, and its excess with respect to x_0 is then advected away from the reaction zone, leading to the expansion of a second traveling front of a more concentrated solution of X invading the bulk. This is seen as a darker disk of radius r_X invading the less concentrated outer zone on Fig. 1(a), top panel [see also Fig. 3(a)]. Similarly, when $x_0 > n$ [Figs. 1(d) and 1(e)], continuous feeding of Y induces an invasion of the reactor by the reactant which consumes X up to a stationary position r_S where the reaction zone freezes and $x = ny$. Beyond this position, the less concentrated solution of X dynamically produced in the frozen front is advected away, leading to the expansion in the bulk of a lighter disk of radius r_X [Fig. 1(a), bottom panel]. Figure 1(f) shows that, in some region around the reaction front, the concentration profiles x and y are independent of x_0 and are fixed by n.

These dynamics can be described analytically in both $t \ll 1$ and $t \gg 1$ asymptotic limits. At early times, the mixing between X and Y is negligible, and the production rate x^2y can be neglected in Eqs. (2) [17,19]. The resulting conservative equations admit a self-similar solution

$$\chi(r,t) = a + b\,\Gamma(Q/2, r^2/(4t)), \tag{3}$$

where Γ is the incomplete gamma function, a and b are arbitrary constants, and $\chi = x$ or y [18,27]. Given the BCs at

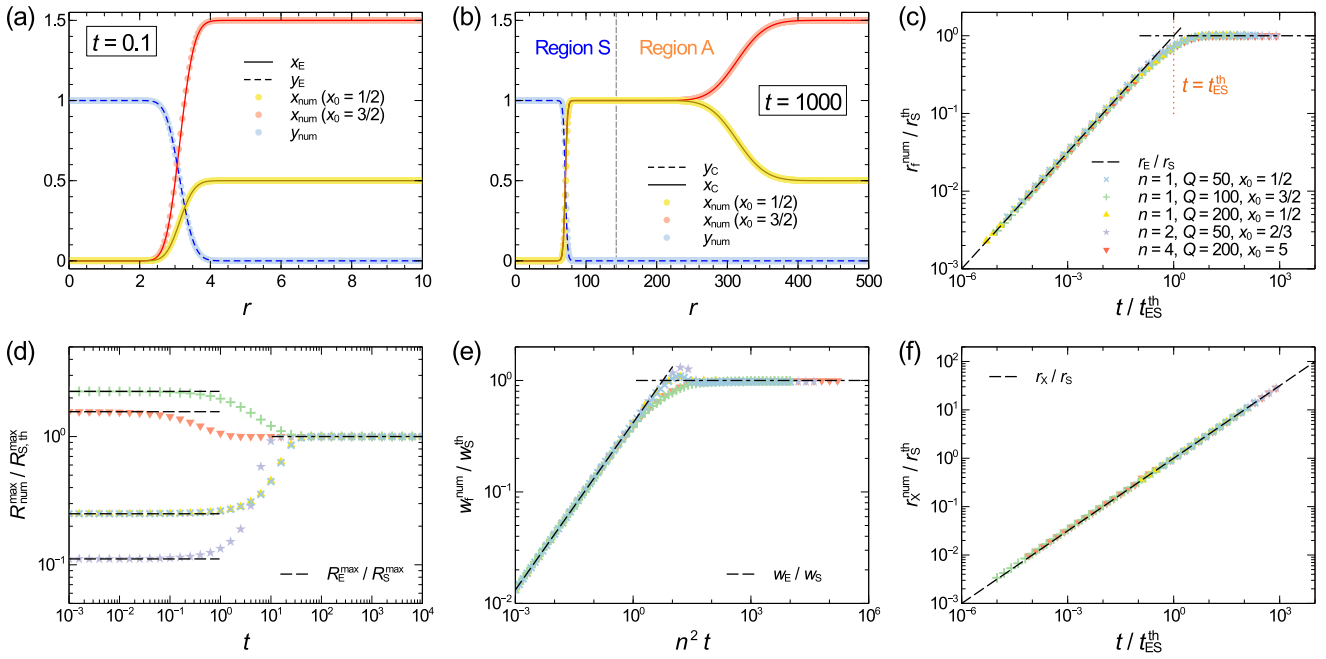

FIG. 2. Numerical concentration profiles, x and y for $n = 1$ and $Q = 50$, compared to the analytical expressions (4) at early times (a) and (14) at long time (b). (c)–(f) The symbols correspond to the numerical evolution of the position r_f (c), amplitude of reaction rate $R^{\max}$ (d), width w_f of the reaction front (e), and position of the advective front r_X (f), all rescaled by their theoretical stationary value, as a function of (rescaled) times. The dashed curves represent the analytical early-time expressions, (c) Eq. (5), (d) Eq. (6), (e) Eq. (7), and (f) Eq. (9), whereas the dashed-dotted curves in (c)–(e) represent their stationary values, (c) Eq. (12) and (d), (e) Eq. (15).

$r = 0$ and $r \to \infty$ for x and y, we get

$$x_E = x_0\left[1 - \mathcal{Q}\left(\frac{Q}{2}, \frac{r^2}{4t}\right)\right], \quad y_E = n\,\mathcal{Q}\left(\frac{Q}{2}, \frac{r^2}{4t}\right), \tag{4}$$

where the index E stands for early times and $\mathcal{Q}(a,\cdot) = \Gamma(a,\cdot)/\Gamma(a)$ is the regularized gamma function [27]. Figure 2(a) shows that Eqs. (4) describe nicely the numerical solutions when t is small enough ($t \ll t_{ES}$, see below). The front position, where the concentration of both species is equal $\bar{x}_E = \bar{y}_E$ ($n\bar{x}_E = \bar{y}_E$), is then given by

$$r_E = 2\left[\mathcal{Q}^{-1}\left(\frac{Q}{2}, \frac{x_0}{1+x_0}\right)t\right]^{\frac{1}{2}} \underset{Q\gg 1}{=} \sqrt{2Qt}. \tag{5}$$

Using Eq. (4), the position, $r_E^{\max}$, of the maximum of the production rate $R_E = x_E^2 y_E$ and its value, $R_E^{\max}$, are easily obtained [28]:

$$r_E^{\max} = 2\left[\mathcal{Q}^{-1}\left(\frac{Q}{2}, \frac{1}{3}\right)t\right]^{\frac{1}{2}}, \quad R_E^{\max} = \frac{4x_0^2 n}{27}. \tag{6}$$

The position of $R_E^{\max}$ is located ahead of the front position r_E when $x_0 > 1/2$ and behind it when $x_0 < 1/2$. However, this difference becomes negligible at large Q as $r_E^{\max} = \sqrt{2Qt}$ in this limit. The front width, w_E, defined as the width at the half height of the production rate R_E, can then be computed using Eq. (4) as

$$w_E(t) = 2\Theta(Q)\,t^{1/2} \underset{Q\gg 1}{=} 1.78\,t^{1/2}, \tag{7}$$

where Θ is given in the Supplemental Material [28]. At any given time, w_E is larger than the width obtained upon injecting the autocatalyst X into the reactant Y, but they become identical at large Q [17].

At long times, the reactor can be separated in two regions [Fig. 1(f)]. In region A, far enough from the reaction front, $y = 0$ so that Eq. (2b) is identically satisfied and Eq. (2a) reduces to the same conservative equation as in the early-time regime with the self-similar solution (3). Ignoring region S for the moment, the BCs $x(0,t) = n$ and $x(\infty,t) = x_0$ lead to

$$x_A = x_0 + (n - x_0)\mathcal{Q}(Q/2, r^2/4t), \quad y_A = 0. \tag{8}$$

If the position r_X of the advected x front is defined as the position where $x = (n + x_0)/2$ [see Figs. 1(b)–1(e)], Eq. (8) gives

$$r_X = 2\left[\mathcal{Q}^{-1}\left(\frac{Q}{2}, \frac{1}{2}\right)t\right]^{\frac{1}{2}} \underset{Q\gg 1}{=} \sqrt{2Qt} \simeq r_E. \tag{9}$$

When $x_0 < n$, this definition holds only at a sufficiently large time when the local maximum of x near the reaction zone is high enough [Fig. 1(b)]. In region S, we note that adding Eqs. (2a) and (2b) yields again a conservative equation for $f = x + y$. Ignoring region A, the BCs to apply to the solution (3) are $x(0,t) = y(\infty,t) = 0$ and $x(\infty,t) = y(0,t) = n$, i.e., $f(0,t) = f(\infty,t) = n$, leading to $a = n$ and $b = 0$. This implies that, in region S, $f(r,t) = x(r,t) + y(r,t) = n$ such that a stationary solution of Eq. (2b) is a solution of

$$d_\xi^2 y - \frac{Q-1}{\xi + r_S} d_\xi y - (n-y)^2 y = 0, \tag{10}$$

with $y(0) = n$ and $y(\infty) = 0$ and $\xi = r - r_S$ where r_S is the stationary front position. Figure 1(f) shows that y is equal to its

boundary values everywhere except in a region around $\xi = 0$, i.e., $r = r_S$. Therefore, ξ can be neglected in front of r_S in Eq. (10) provided $r_S \gg 1$. The resulting autonomous equation is a classical traveling wave equation with solution [6]

$$y_S = n\,\frac{e^{-c(r-r_S)}}{1+e^{-c(r-r_S)}}, \quad x_S = n - y_S, \tag{11}$$

provided $c \equiv (Q-1)/r_S = n/\sqrt{2}$, which gives

$$r_S = \frac{Q\sqrt{2}}{n}, \quad \bar{r}_S = \frac{\bar{Q}\sqrt{2}}{2n\pi\bar{h}\bar{y}_0\sqrt{\bar{D}\bar{k}}}, \tag{12}$$

where we have used $Q \gg 1$ since we have assumed $r_S \gg 1$. Note that r_S can also be obtained by equating the radial advection speed, $v_r = Q/r$, with the traveling wave speed $c = n/\sqrt{2}$. The time t_{ES} at which the front becomes frozen can be estimated from the relation $r_E = r_S$ leading to

$$t_{ES} = Q/n^2, \quad \bar{t}_{ES} = \frac{\bar{Q}}{2\pi n^2\bar{h}\bar{D}\bar{k}\bar{y}_0^2}. \tag{13}$$

A composite solution can now be constructed by adding the solutions in each region S and A and subtracting their common part in the overlapping region,

$$y_C(r) = y_S(r), \quad x_C(r,t) = x_S(r) + x_A(r,t) - n, \tag{14}$$

provided $r_X \simeq r_E \gg r_S$, i.e., $t \gg t_{ES}$. Figure 2(b) shows that Eq. (14) describes nicely the numerical solutions of Eqs. (2) at large times. Finally, the position, $r_S^{\max}$, amplitude, $R_S^{\max}$, and width, w_S, of the stationary reaction rate, $R_S = x_S^2 y_S$, located in the region S can be obtained by using Eq. (11) [28]:

$$r_S^{\max} = r_S + \frac{\sqrt{2}\ln 2}{n}, \quad R_S^{\max} = \frac{4n^3}{27}, \quad w_S \simeq \frac{4.26}{n}. \tag{15}$$

Figures 2(c)–2(f) compare the evolution of r_f, $R^{\max}$, w_f, and r_X computed from the numerical solutions of Eqs. (2) to their corresponding analytical expressions at early and long times. In all cases, very nice agreement is observed.

To test the theory, experiments are performed using the CT reaction where $n = 6$, $\bar{D} = 9.3\times10^{-9}$ m^2 s^{-1}, $\bar{k} = 4\bar{k}'\bar{y}_0$, $\bar{k}' = 1.365\times10^5$ s^{-1} M^{-3} [28]. Figure 3(a) shows a typical stationary front in a quasi-2D reactor. The space-time plot in Fig. 3(b) shows saturation of the position $\bar{r}_f$ of the reaction front to its stationary value $\bar{r}_S$ at large time and the continuous increase of the position $\bar{r}_X$ of the second advected front. Figure 3(c) compares Eq. (12) to the experimental values $\bar{r}_S$ as a function of the flow rate $\bar{Q}$, for various initial concentrations $\bar{y}_0$ and reactor heights $\bar{h}$. We see that $\bar{r}_S\bar{h}\,\bar{y}_0^{3/2} = \alpha\,\bar{Q}$, where $\alpha = [2\sqrt{2}\pi n\sqrt{\bar{D}\bar{k}'}]^{-1} \simeq 0.53$ which describes nicely the data. Similar excellent agreement between theory and experiments is obtained for the temporal evolution of both fronts' position (see Supplemental Material [28]).

To conclude, we have shown, numerically, theoretically, and experimentally, that autocatalytic fronts exposed to a radial injection of the reactant Y into a sea of the autocatalytic species X reach a stationary position due to the competition between inward RD front motion and outward advection. Ahead of this stationary front, adaptation of the outer concentration of the autocatalytic species to the stoichiometry ratio between X and Y induces a second outward traveling front. Analytical solutions for concentration profiles and properties of both stationary and outer traveling fronts have been derived. An excellent agreement between theoretical predictions and experiments using the chlorite-tetrathionate reaction is demonstrated. Further work could exploit the stationarity of the chemical front to study stationary patterns due to various instabilities.

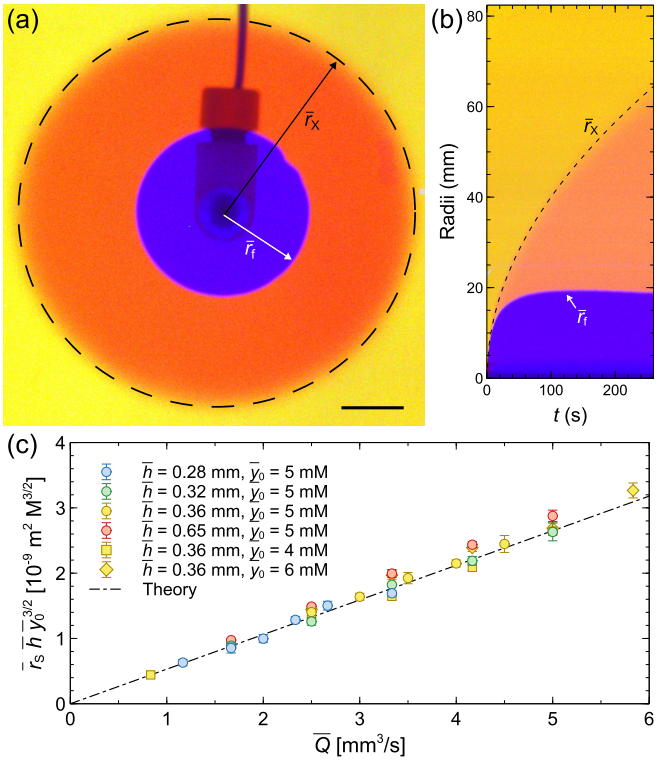

FIG. 3. (a) Experimental stationary and outward traveling fronts in the CT autocatalytic reaction shown at $\bar{t} = 325$ s obtained when the blue Y solution ($\bar{y}_0 = 6$ mM) is injected into the yellow pool of X ($\bar{x}_0 = 12$ mM $< n\bar{y}_0$) with $\bar{Q} = 200$ μL min^{-1} and $\bar{h} = 0.36$ mm. Scale bar: 10 mm. (b) Space-time plot of the dynamics along a radial line of (a). The zone of higher concentration of X (lower pH, orange) spreads into the zone of lower concentration of X (higher pH, yellow). (c) Rescaled stationary front position $\bar{r}_S\bar{h}\,\bar{y}_0^{3/2}$ as a function of the flow rate $\bar{Q}$ for different reactant concentrations $\bar{y}_0$ and reactor heights $\bar{h}$. The symbols represent experimental results, and the dashed line is the theoretical prediction (12).

We thank S. N. Maharana for fruitful discussions. This project has received funding from the European Union's Horizon 2020 research and innovation programme under the Marie Skłodowska-Curie Grant Agreements No. 801505 and No. 956457.

A. Comolli's present affiliation is the European Research Council Executive Agency. The views expressed are purely those of the authors and may not in any circumstances be regarded as stating an official position of the ERCEA and the European Commission.

[1] J. D. Murray, *Mathematical Biology* (Springer, New York, 1989), Vol. 17.

[2] I. R. Epstein and J. A. Pojman, *An Introduction to Nonlinear Chemical Dynamics* (Oxford University Press, Oxford, UK, 1998).

[3] *Chemical Waves and Patterns*, edited by R. Kapral and K. Showalter (Springer, Amsterdam, 1995).

[4] N. Ahmed, A. Elsonbaty, A. Raza, M. Rafiq, and W. Adel, Numerical simulation and stability analysis of a novel reaction–diffusion COVID-19 model, Nonlin. Dyn. **106**, 1293 (2021).

[5] R. Tiani, J. A. Pojman, and L. Rongy, Critical role of layer thickness in frontal polymerization, J. Phys. Chem. B **126**, 3607 (2022).

[6] R. Fisher, The wave of advance of advantageous genes, Ann. Eugen. **7**, 355 (1937).

[7] S. K. Scott, *Oscillations, Waves, and Chaos in Chemical Kinetics* (Oxford University Press, Oxford, UK, 1994).

[8] Á. Tóth, D. Horváth, and A. Siska, Velocity of propagation in reaction-diffusion fronts of the chlorite-tetrathionate reaction, J. Chem. Soc. Faraday Trans. **93**, 73 (1997).

[9] M. Abel, A. Celani, D. Vergni, and A. Vulpiani, Front propagation in laminar flows, Phys. Rev. E **64**, 046307 (2001).

[10] T. D. Nevins and D. H. Kelley, Front tracking velocimetry in advection-reaction-diffusion systems, Chaos **28**, 043122 (2018).

[11] B. F. Edwards, Poiseuille advection of chemical reaction fronts, Phys. Rev. Lett. **89**, 104501 (2002).

[12] M. Leconte, J. Martin, N. Rakotomalala, and D. Salin, Pattern of reaction diffusion fronts in laminar flows, Phys. Rev. Lett. **90**, 128302 (2003).

[13] T. D. Nevins, D. E. Troyetsky, and D. H. Kelley, Efficient autocatalytic reactive mixing and solitary chemical waves in laminar flows, Phys. Rev. Fluids **5**, 063201 (2020).

[14] S. Atis, S. Saha, H. Auradou, D. Salin, and L. Talon, Autocatalytic reaction fronts inside a porous medium of glass spheres, Phys. Rev. Lett. **110**, 148301 (2013).

[15] S. Saha, S. Atis, D. Salin, and L. Talon, Phase diagram of sustained wave fronts opposing the flow in disordered porous media, Europhys. Lett. **101**, 38003 (2013).

[16] T. Chevalier, D. Salin, and L. Talon, Frozen fronts selection in flow against self-sustained chemical waves, Phys. Rev. Fluids **2**, 043302 (2017).

[17] A. Comolli, L. Negrojević, F. Brau, and A. De Wit, Effect of radial advection on autocatalytic reaction–diffusion fronts, Phys. Chem. Chem. Phys. **25**, 10604 (2023).

[18] F. Brau, G. Schuszter, and A. De Wit, Flow control of $A + B \rightarrow C$ fronts by radial injection, Phys. Rev. Lett. **118**, 134101 (2017).

[19] A. Comolli, A. De Wit, and F. Brau, Dynamics of $A + B \rightarrow C$ reaction fronts under radial advection in three dimensions, Phys. Rev. E **100**, 052213 (2019).

[20] Á. Tóth, G. Schuszter, N. P. Das, E. Lantos, D. Horváth, A. De Wit, and F. Brau, Effects of radial injection and solution thickness on the dynamics of confined $A + B \rightarrow C$ chemical fronts, Phys. Chem. Chem. Phys. **22**, 10278 (2020).

[21] P. Karan, U. Ghosh, F. Brau, Y. Méheust, and T. Le Borgne, Effect of hydrodynamic dispersion on spherical reaction front dynamics in porous media, Phys. Rev. Fluids **8**, 084502 (2023).

[22] M. Dentz, T. Le Borgne, A. Englert, and B. Bijeljic, Mixing, spreading and reaction in heterogeneous media: A brief review, J. Contam. Hydrol. **120-121**, 1 (2011).

[23] E. Guilbert, C. Almarcha, and E. Villermaux, Chemical reaction for mixing studies, Phys. Rev. Fluids **6**, 114501 (2021).

[24] A. De Wit, Chemo-hydrodynamic patterns and instabilities, Annu. Rev. Fluid Mech. **52**, 531 (2020).

[25] A. D. C. Nguindjel, P. J. de Visser, M. Winkens, and P. A. Korevaar, Spatial programming of self-organizing chemical systems using sustained physicochemical gradients from reaction, diffusion and hydrodynamics, Phys. Chem. Chem. Phys. **24**, 23980 (2022).

[26] A. Hanna, A. Saul, and K. Showalter, Detailed studies of propagating fronts in the iodate oxidation of arsenous acid, J. Am. Chem. Soc. **104**, 3838 (1982).

[27] F. W. Olver, D. W. Lozier, R. Boisvert, and C. W. Clark, *The NIST Handbook of Mathematical Functions* (Cambridge University Press, Cambridge, UK, 2010).

[28] See Supplemental Material at http://link.aps.org/supplemental/10.1103/PhysRevResearch.6.L042044 for additional calculations, detailed descriptions of experimental procedures, and experimental results regarding the dynamics of the front position.